Post-Print of an Accepted Manuscript on the Laboratory of Turbulent Flows Website

The Accepted Manuscript begins on the next page.

A modular, 3D-printed helium-filled soap bubble generator for large-scale volumetric flow measurements

Bradley Gibeau[1] and Sina Ghaemi[1]†

[1] Department of Mechanical Engineering, University of Alberta, Edmonton, Alberta T6G 2R3, Canada
† ghaemi@ualberta.ca

Abstract

A modular helium-filled soap bubble (HFSB) generator consisting of 3D-printed nozzles and developed for use in a wind tunnel is characterized. A multi-syringe pump accurately feeds bubble film solution (BFS) to each nozzle while air and helium flow rates are regulated using mass flow controllers. The modular design of the system allows for the customization of the HFSB streamtube to each unique experiment. Modules can be arranged in various configurations to increase seeding density and manipulate the size of the streamtube. Shadowgraphy, particle image velocimetry (PIV), particle tracking velocimetry (PTV), and laser-based imaging are used to characterize the particle sizes, tracing fidelity, production rates, and seeding density of a system consisting of two modules (8 nozzles in total). It is shown that nozzle performance, particle time response, and production rates can be controlled by varying the flow rates of air, helium, and BFS into the system, respectively. The optimal operating case resulted in the production of approximately 70,000 bubbles/s from each nozzle. The bubbles were neutrally buoyant on average and had a mean diameter of 0.46 mm. The two modules resulted in a streamtube with an effective cross-section of 15×15 cm^2. The streamtube was produced continuously, resulting in a seeding density of 1.6 bubbles/cm^3 at free stream velocity of 10.3 m/s.

1 Introduction

Particle image velocimetry (PIV) and particle tracking velocimetry (PTV) have become staples for measuring fluid flows due to the non-invasive nature of the measurement and the resulting high-density data. In the last decade, these techniques have been extended to carry out volumetric measurement with high spatial resolution (Elsinga et al. 2006; Schanz et al. 2016). Seeding the flow with particles that scatter sufficient light while remaining faithful to the flow field is crucial for ensuring measurement quality. However, fulfilling both criteria is a challenge, especially for volumetric measurements. The amount of light scattered by a particle increases with particle diameter (Raffel et al. 2007), but inertial effects cause large, heavy particles to lag behind the true flow field. Standard particles used for particle velocimetry in air have diameters on the order of 1 μm. While these particles exhibit high tracing fidelity, their light scattering ability limits volumetric measurements to the order of 10 cm^3 with current imaging and illumination technology (Scarano 2013). This allows for highly detailed analyses of small-

scale flow features, but there are limitations for applications that require full-scale wind tunnel tests with large measurement volumes. Moreover, the available light energy can limit the measurement to even smaller volumes when performing time-resolved measurements using high-speed lasers.

The use of helium-filled soap bubbles (HFSBs) as tracer particles has been gaining popularity recently for their potential to allow for volumetric measurements on the order of 1 m^3. The bubbles have diameters on the order of 1 mm and can be made neutrally buoyant in air, resulting in ideal flow tracing. HFSBs were first used for flow visualization experiments (eg. Hale et al. 1971), and the first thorough characterization of their tracing fidelity was performed by Kerho and Bragg (1994). A commercial HFSB generator was used to produce bubbles with diameters ranging from 1-5 mm, which were then filtered through a vortex filter to remove the heavier-than-air particles. The filtered particles were tracked in the stagnation region of a NACA airfoil and compared to the streamlines of an equivalent potential flow. It was found that the particle tracks deviated from the calculated streamlines, and this was

attributed to the particles not being neutrally buoyant. In this case, the vortex filter did not remove the lighter-than-air particles. The authors concluded that the use of HFSBs should be limited to qualitative analyses unless care is taken to ensure neutral buoyancy.

A more recent experiment conducted by Scarano et al. (2015) measured HFSBs near the stagnation region of a circular cylinder in a wind tunnel at a freestream velocity of 30 m/s. The flowrates of helium and soap into a HFSB nozzle were tuned to obtain particles that were nearly neutrally buoyant with a relaxation time two orders of magnitude less than the characteristic time scale of their flow and with a diameter of 0.4 mm. PIV and PTV were used to compare particle velocities to those obtained using standard 1-µm particles, and the authors concluded that the particles were suitable for quantitative flow measurements. This demonstrated that current HFSB generators are capable of producing bubbles with sufficient tracing fidelity for flow measurements when neutral buoyancy can be ensured.

HFSBs have been successfully used for particle velocimetry in a variety of experiments. Müller et al. (2001) used particle-streak tracking (PST) to conduct three-dimensional velocity measurements at the inlet of a heat exchanger. Bosbach et al. (2009) performed large-scale PIV in the cross-section of a full-scale aircraft cabin. Kühn et al. (2011) performed large-scale tomographic-PIV of a convection cell in a volume of roughly 0.06 m^3 and provide a detailed treatment of the associated challenges. Scarano et al. (2015) illuminated a volume of 0.01 m^3, with half that being used for a tomographic-PIV measurement. To the authors' knowledge, the largest volumetric measurement to date was performed by Huhn et al. (2017), where particle tracking (shake-the-box) was used to measure a thermal plume with a volume of 0.56 m^3 within an enclosure. HFSBs have also been used to develop specialized particle tracking algorithms (Biwole et al. 2009), extract quantitative data from visualizations using grids (Babie and Nelson 2010), measure large-scale volumetric pressure fields (Schneiders et al. 2016), improve vortex core velocimetry measurements (Caridi et al. 2017), estimate drag on a towed sphere (Terra et al. 2017), and study wall-bounded turbulence (Engler Faleiros et al. 2018).

Despite the large amount of recent success in experiments using HFSBs, seeding the flow with a sufficient number of particles still poses a large challenge. The best HFSB nozzles currently available produce bubbles at rates that are much lower than what is required for proper seeding in a wind tunnel environment (Caridi et al. 2016), where particles are constantly being carried away from the measurement region. Until now, this issue has been mitigated by performing measurements in enclosed spaces (Bosbach et al. 2009, Kühn et al. 2011, Huhn et al. 2017, Terra et al. 2017), tracking sparse amounts of particles (Kerho and Bragg 1994, Müller et al. 2001, Caridi et al. 2017, Engler Faleiros et al. 2018), or collecting and releasing particles into the flow for a short burst (~1 second) of high-density seeding (Scarano et al. 2015, Caridi et al. 2016). In the latter case, a piston-cylinder system was used to collect the particles before a controlled release into the flow through an aerodynamic rake. In the experiment by Caridi et al. (2016), this resulted in a successful tomographic-PIV measurement within a wind tunnel with a volume of 0.024 m^3. While this represents significant progress in the development of HFSB systems, the authors reported a production rate that was 1/3 what they had predicted, and they attributed this primarily to bubble destruction within the release system. They suggested that a multi-nozzle system that can produce sufficient numbers of HFSBs directly in the stream of the wind tunnel has the potential to overcome the issues associated with the piston-cylinder system.
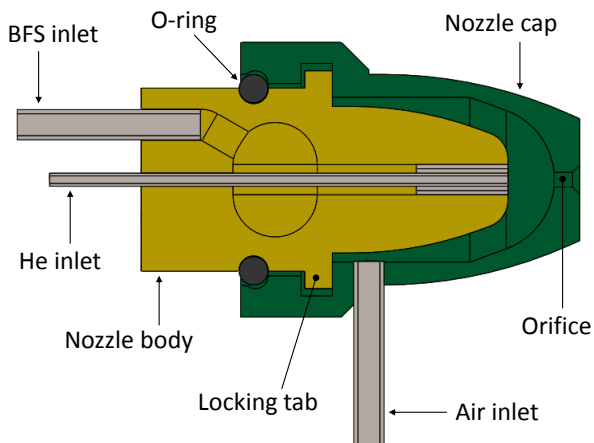
Considering the seeding issues described here, this work focuses on the development and characterization of a HFSB system that makes use of multiple nozzles to produce bubbles directly into a wind tunnel. The system is based entirely around 3D-printed components, readily available parts, and standard lab equipment. The design of a single nozzle is detailed and the full-scale system used within a wind tunnel environment is outlined. The system features a modular design, where individual blocks can be arranged to tailor the HFSB streamtube to each experiment by varying the seeding density and the size of the streamtube cross-section. Shadowgraphy, PIV, PTV, and laser-based imaging experiments are used to characterize the particle sizes, tracing fidelity, production rates, and seeding density of the HFSBs from the system. The impact of varying air, helium, and bubble film solution (BFS) flow rates into the nozzles is determined.

2 The Helium-Filled Soap Bubble Generator

2.1 Nozzle Design

The nozzle was developed iteratively beginning with descriptions provided by Bosbach et al. (2009). The authors discussed two types of nozzles: pitot-tube-type nozzles and orifice-type nozzles. Pitot-tube-type nozzles are composed of three concentric flow tubes. The inner tube supplies helium which is blown through BFS injected by the second tube. The outermost tube provides a flow of air that acts to detach the concentric flow from the end of the nozzles to form bubbles. Similarly, orifice-type nozzles utilize two concentric tubes to provide helium and BFS. In contrast, the air flow is supplied to a chamber around the nozzle with a small opening (i.e. the orifice). Bubbles formed at the end of the tubes are forced to contract and detach upon entering the orifice. As indicated by Bosbach et al. (2009), the orifice-type nozzle was found to be superior due to its higher production rates and improved control over bubble sizes, thus having a better chance at achieving neutral buoyancy. Consequently, we have moved forward focusing on the orifice-type nozzle.

The construction of the present HFSB nozzle can be viewed in Fig. 1. The two primary nozzle components, the body and the cap, were developed using a Formlabs 3D printer (Form 2). The nozzle body and cap are secured together by two locking tabs that are detailed in Fig. 1. The tabs slide into axial grooves in the cap which lead to a ring groove. Turning the cap then locks the two pieces together (sealed by an o-ring). Stainless steel tubing and a syringe needle were used in addition to the 3D-printed components to create consistent and smooth paths for the helium, air, and BFS. These components are necessary for overcoming the large tolerances associated with 3D printing, which can lead to inconsistent results. The flow tube for helium consists of a blunt 22-guage syringe needle (OD = 0.71 mm, ID = 0.48 mm). The remaining tubes for air and BFS are made of 16-gauge stainless steel tubing (OD = 1.65 mm, ID = 1.35 mm), which are attached to the body using an adhesive. The exit orifice at the end of the cap has a diameter of 0.8 mm. The orifice was printed smaller than 0.8 mm and enlarged to the proper dimension using precision tools to ensure consistent orifice diameters between nozzles.

When testing the nozzles, it was noticed that they operated inconsistently when oriented horizontally. This was primarily due to BFS building up within the nozzle cap, leading to sputtering and sometimes complete nozzle shutdown. Tests with nozzles oriented vertically pointing downwards led to a vast improvement in nozzle operation, resulting in constant bubble production without interruption. This is likely due to gravity assisting the axisymmetry of the three concentric flows, as well as the ability of the nozzle to drain of BFS if a buildup were to occur. We decided to implement the nozzles into the system vertically for this reason.

2.2 Full-Scale System

The full-scale HFSB system in the present study consists of two block-shaped modules. As shown in Fig. 2, each module features 4 nozzles mounted vertically at the top of a 3D-printed square duct with dimensions 20×15×15 cm^3 (*L×W×H*) and a wall thickness of 3 mm. Although two ducts are arranged side-by-side in the present experiments, the system allows for different configurations. The primary idea behind the design is (i) the ability to increase seeding density by aligning nozzles in series within a module, and (ii) to customize the shape of the streamtube cross-section by stacking several modules in different side-by-side arrangements. This allows for the tailoring of the HFSB streamtube to each unique wind tunnel experiment. Moreover, the resulting honeycomb-like structure of the modules with thin walls leads to reduced upstream flow disruption and possible integration into the wind tunnel honeycomb structure.

The HFSB nozzles require a source of helium, air, and BFS. A canister of compressed helium provided a helium flow, which was controlled using a 0.1-10

Fig. 1 Schematic of the 3D-printed nozzle, stainless steel tubing, and syringe needle.

Fig. 2 Components of the full-scale system. (*a*) Annotated photograph of the two-module HFSB generator. (*b*) Front view of the HFSB generator; each module has dimensions 20×15×15 cm³. (*c*) The multi-syringe pump used to regulate BFS to each of the 8 nozzles.

L/min digital flow controller (Cole-Parmer, model # 32907-71). The flow rate of compressed air was controlled using a second 0.1-10 L/min controller of the same make and model. Each of the gas flows passed through a separate axisymmetric distribution system to promote equal flow rates to the nozzles. A multi-syringe pump (World Precision Instruments, AL-8000) was used to provide a dedicated flow of BFS (Sage Actions Inc., 1035) to each nozzle and is shown in Fig. 2. Considering the volume of compatible syringes (~10 mL) and typical values for $\dot{V}_{\text{BFS}}$ (<10 mL/hr), the full-scale system can run continuously for longer than an hour. The different flow rates of helium ($\dot{V}_{\text{He}}$), air ($\dot{V}_{\text{air}}$), and BFS ($\dot{V}_{\text{BFS}}$) to each nozzle are given in Table 1. Every combination was tested, resulting in 36 operating cases.

The full-scale experiments were conducted at free stream velocity 10.3 m/s in a two-story, closed-loop wind tunnel at the University of Alberta. The test section is located after a 6.3:1 contraction and has cross-sectional dimensions of 2.4 × 1.2 m² (*W*×*H*). The maximum turbulence intensity at the midpoint of the test section has been measured to be 0.4% (Johnson & Kostiuk 2000). An aluminum circular cylinder with a diameter of 50 mm was oriented vertically 7.3 m downstream from the HFSB generator, which was located within the settling chamber of the wind tunnel as depicted in Fig. 3.

3 Characterization of the System

Three experiments were necessary for full characterization of the modular HFSB system. These included shadowgraphy, PIV/PTV, and laser-based

imaging and were used to measure bubble sizes, time responses, production rates, and seeding densities. These experiments are shown schematically in Fig. 4 and are described next.

3.1 Shadowgraphy

The shadowgraphy experiments (*x-y* plane in Fig. 4) required a high magnification, and so the HFSB streamtube was moved close to the wall of the test section and the illumination optics were moved into the test section to improve the magnification of the images. A reduced free stream velocity of roughly 4 m/s was used during these experiments to increase the number of HFSBs captured by the high-magnification images. Illumination for the experiment was provided by a dual-cavity Nd:YAG laser (New Wave Research, Solo PIV III) capable of producing 532 nm light at 50 mJ per pulse (at 15 Hz repetition rate). The laser beam was directed into a diffusor to obtain the necessary backlight illumination for shadowgraphy. An Imager ProX-4M camera was used to collect images. The camera features a 2048×2048-pixel (7.4×7.4 μm² pixel size) CCD sensor and 14-bit resolution. A 200-mm Nikon lens with an aperture setting of *f*/32 was used to obtain a FOV of 21×21 mm² and a resolution of 10.4 μm/pix. Sets of 2000 single-frame images were collected at a rate of 10 Hz for all cases considered, and the resulting data sets were processed using the particle sizing feature of DaVis 8.4 (LaVision GmbH). A minimum centricity of 85% was enforced, and a wide range of particle sizes were permitted to be measured to ensure that the algorithm was not selective.
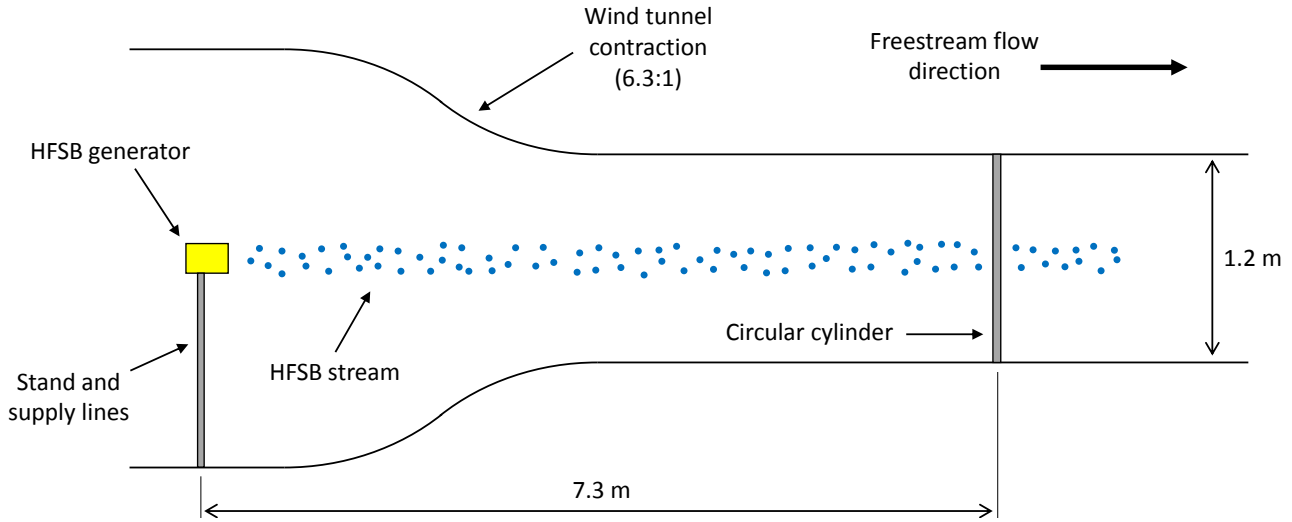
4

Fig. 3 Overview of the experimental configuration.

3.2 Particle Image/Tracking Velocimetry

A two-component PIV/PTV measurement was utilized in the front stagnation region of the circular cylinder (x-z plane in Fig. 4) to measure the dynamics of the base flow using standard 1-μm particles and of the HFSBs. The base flow was measured using a reduced FOV compared to that of the HFSB experiments due to lack of contrast in the images using standard 1-μm particles. Illumination at 527 nm was generated using a dual-cavity Nd:YLF laser (Photonics Industries, DM20-527-DH) which is capable of producing 527 nm light at 20 mJ per pulse (at 1 kHz repetition rate). The laser beam was directed using several adjustable mirrors before being formed into a sheet with a thickness of 2 mm using a combination of spherical and cylindrical lenses. A high-speed camera (Phantom, v611) with a 1280×800-pixel (20×20 μm^2 pixel size) CMOS sensor and 12-bit resolution was used to collect images. A 200-mm Nikon lens with an aperture setting of f/4 was used to obtain a FOV of 93×58 mm^2 for PIV using the 1-μm fog droplets (resolution of 72.6 μm/pix). A 105-mm Nikon lens with an aperture setting of f/2.8 was used to obtain an enlarged FOV of 203×203 mm^2 (cropped) for PIV/PTV using the HFSBs (resolution of 253 μm/pix). The lower magnification of the imaging system in the latter case prevented the formation of doublet patterns in the HFSB images. To aid convergence, 15 cycles of images were collected over the course of 15 seconds for all PIV/PTV experiments. A total of 2400 double-frame images were collected at a rate of 500 Hz when using fog droplets. For all HFSB sets, 7500 time-resolved images were collected at a rate of 5 kHz. DaVis 8.4 was used to apply a sum-of-correlation (Meinhart et al. 2000) with 32×32-pixel interrogation windows to all sets, leading to a time-averaged vector field in all cases. The time-resolved 2D-PTV algorithm within DaVis 8.4 was also applied to select cases of time-resolved HFSB data in addition to the sum-of-correlation to obtain individual particle velocities. Particles were detected using a Gaussian 3×3 fit with an intensity threshold of
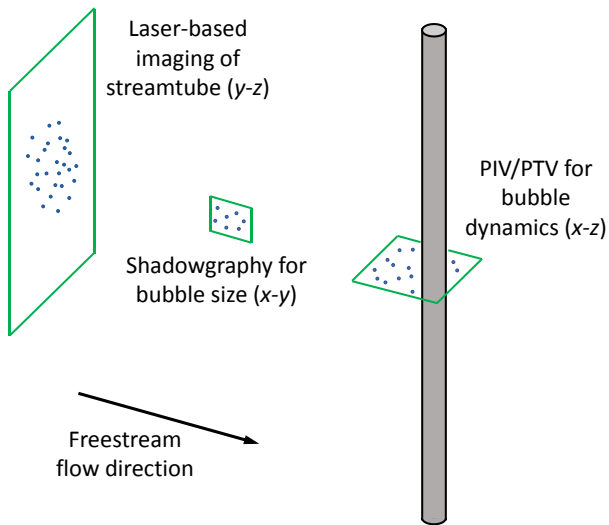

Fig. 4 Viewing regions for all experiments in the present investigation.

Table 1 Flow rates of air, helium, and BFS considered during experiments (values are per nozzle).

| $\dot{V}_{air}$ [L/min]	$\dot{V}_{He}$ [L/min]	$\dot{V}_{BFS}$ [mL/hr]
0.7, 0.9, 1.1	0.06, 0.12, 0.18, 0.24	4, 6, 8

50 counts, and all particle tracks with lengths of less than 5 were discarded.

3.3 Imaging of the Streamtube Cross-Section

Snapshots of the streamtube cross-section (y-z plane in Fig. 4) were taken to count the number of particles produced by the HFSB generator. The same laser and camera utilized for the PIV/PTV experiments were applied here. The laser sheet was once again made to be 2 mm thick using a combination of spherical and cylindrical lenses, and it was large enough to capture the entire HFSB streamtube. A 105-mm Nikon lens with an aperture setting of f/8 was used to obtain a FOV of 492×303 mm^2. The camera was set at an angle of 20° with the floor of the wind tunnel and so a target calibration was necessary for correcting perspective, resulting in a resolution of 363 µm/pix. A set of 500 single-frame images was collected over 20 seconds for each case considered. An in-house 2D peak counting code was used to determine the number of particles within each snapshot.   The average number of particles within the collected images can be used along with the known laser sheet thickness (2 mm) and flow velocity (10.3 m/s) to estimate HFSB production rates and seeding densities. The thickness of the laser sheet was measured using millimeter grid paper. The light passed through the paper and the thickness was read on the back side where only the intense portion of the Gaussian light distribution was visible.

It is possible to overestimate the number of particles within the laser sheet using this method because of the large size of the HFSBs. A particle that is partially within the laser sheet can still emit light and has the potential to be detected by the camera sensor. As will be evident in Section 4.1, the HFSBs have mean diameters on the order of 0.5 mm in most cases. Adding this dimension to both sides of the laser sheet leads to a maximum effective measurement depth-of-field of approximately 3 mm. This effective thickness has been used when estimating production rates and seeding densities.

A threshold was employed when counting particles from the images so that dimmer particles were neglected. These dimmer particles may have been generated by the tails of the Gaussian light intensity distribution or smaller bubbles. The threshold has been chosen as an intensity count of 150 by inspection of multiple image samples. A 6×6-cm^2 segment of one of the raw images within the y-z plane is shown in Fig.
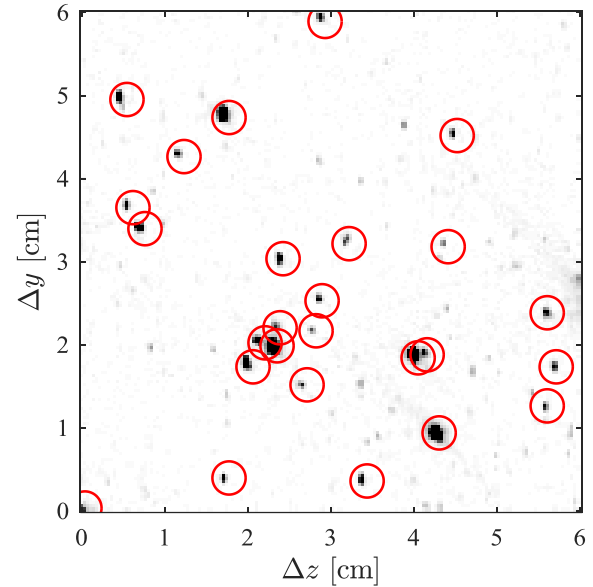
Fig. 5. Sample 6×6-cm^2 segment of a snapshots in the y-z plane (Fig. 4) used to count the number of particles in the streamtube. The red circles mark the particles that have been counted by the 2D peak counting code. All particles with peak counts of less than 150 have been neglected.

5, where the red circles indicate the particles that have been counted by the in-house code. The dimmer particles are neglected as is visible in the sample.

4 Results and Discussion

4.1 Bubble Size

The mean diameters of the HFSBs ($\bar{d}_{HFSB}$) for all 36 operating cases were determined by applying the particle sizing algorithm in DaVis 8.4 to the high-magnification shadowgraphy images as detailed in Section 3.1. Fig. 6 contains the results, where the error bars represent the standard deviation of each distribution of particle sizes.

Each of the three plots in Fig. 6 represents a different flow rate of air into the nozzles, and each line within a plot represents a different flow rate of BFS. The flow rate of air into the nozzles does not seem to have a large impact on HFSB diameter, but a slight shift of the trends downwards is visible as $\dot{V}_{air}$ is increased. There is a clear separation between the lines in each plot, with an increase in $\dot{V}_{BFS}$ producing a shift upwards. This suggests that $\bar{d}_{HFSB}$ may be increased because of a thicker film of BFS. Finally, the flow rate of helium into each nozzle produces the

largest changes in diameter, and this is expected because the volume of each bubble is primarily comprised of helium.

The standard deviations of $\bar{d}_{\mathrm{HFSB}}$ in Fig. 6 range in
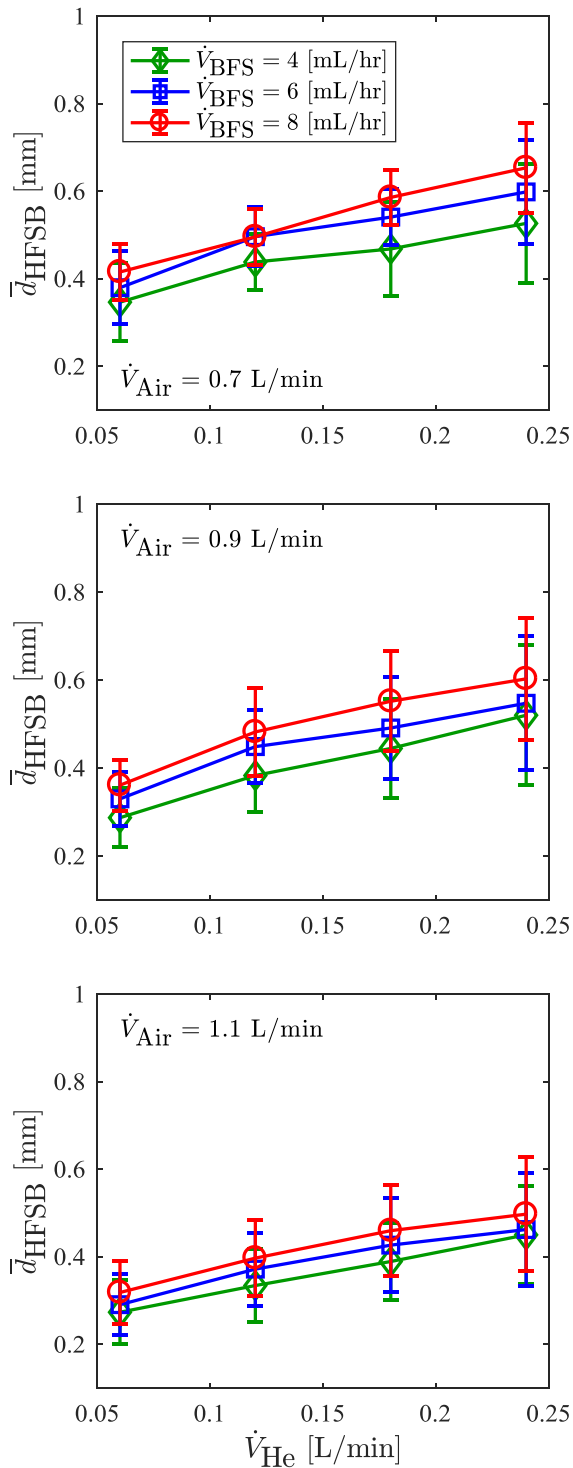
Fig. 6 Mean HFSB diameters ($\bar{d}_{\mathrm{HFSB}}$) for all 36 nozzle operating cases. The error bars represent the standard deviation of each distribution.

value from 11% to 31% of the mean for each respective distribution. These distributions are therefore quite broad in comparison to those presented by Engler Faleiros et al. (2018), who measured the size and time response of HFSBs produced from a single nozzle. The authors reported a mean HFSB diameter of 0.55 mm with a standard deviation of 13%. The broader range of particles measured here may be attributable to the use of multiple nozzles. Minor differences between individual nozzles and the difficulties associated with distributing equal flow rates to each nozzle can result in the production of a wider range of bubbles sizes. Another possible cause of the broad distribution is the operating condition of the nozzles, i.e. downward into a cross-flow. It is not currently known how this configuration affects bubbles production at the exit of the nozzle compared with the horizontal operation of the nozzle. This has been confirmed using the results from a separate shadowgraphy measurement of a single nozzle that was performed during the iterative design phase. Fig. 7 compares distributions of HFSB diameters obtained using a single nozzle and using 8 nozzles with $\dot{V}_{\mathrm{BFS}} = 8$ mL/hr, $\dot{V}_{\mathrm{He}} = 0.18$ L/min, and $\dot{V}_{\mathrm{Air}} = 1.1$ L/min in the current system. Both distributions have a mean of approximately 0.46 mm, but the standard deviations are 10% and 23% for the single and 8-nozzle experiments, respectively.
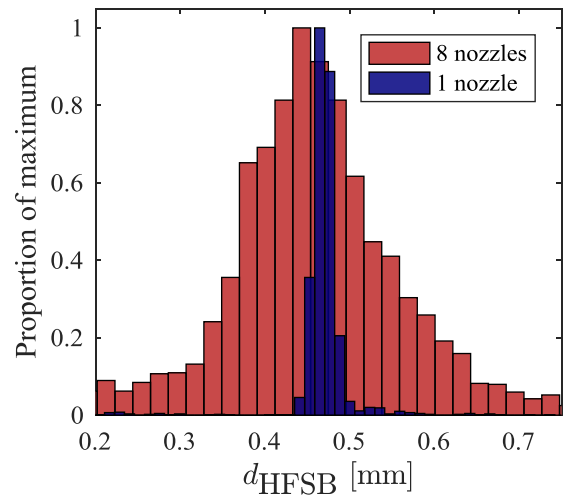
Fig. 7 Distributions of HFSB diameters obtains using a single nozzle and using 8 nozzles in the current system. The mean diameter in both cases is approximately 0.46 mm.

4.2 Bubble Response Time

The tracing fidelity of the HFSBs can be quantified using the measured time response (τ). Assuming a steady flow, the following relationship can be used to estimate the time response of the HFSBs along the stagnation streamline upstream from the cylinder (Scarano et al. 2015, Engler Faleiros et al. 2018):

$$\tau = \frac{u - u'}{u' \frac{\delta u'}{\delta x}} \tag{1}$$

where u is the true streamwise fluid velocity and u' is the streamwise velocity of the HFSBs. In the present analysis, the reference velocity u has been derived from the mean velocity field obtained by applying a sum-of-correlation to the PIV images of the 1-µm fog particles.

It is important to note that Eq. 1 assumes a steady flow field, but the wake of the circular cylinder in the present experiment experiences an unsteady vortex shedding pattern, resulting in some unsteadiness in the upstream flow. The unsteadiness causes a deviation from the mean flow of a few percent in the region of interest, which is negligible when considering averaged flow fields. When considering individual particle tracks from PTV, this slight unsteadiness is expected to artificially broaden the time response distributions by a small amount.

The mean velocity fields from the sum-of-correlation technique applied to both the 1-µm fog particles (to obtain u) and HFSBs (to obtain u') have been used with Eq. 1 to investigate the mean time response ($\bar{\tau}$) of the HFSBs for all 36 cases of nozzle input parameters. The spatial derivative of u' has been calculated by applying a least-squares optimal quadratic fit with a kernel size of 5 to the mean velocity fields. The values for $\bar{\tau}$ have been averaged for each nozzle operating case using all available data along the stagnation streamline in the range $-0.5d \leq x \leq 0$, where $x = 0$ represents the front stagnation point of the circular cylinder. This range was chosen for the large deceleration that occurs leading up to the stagnation point. The results for the mean time responses are plotted in Fig. 8, where $\bar{\tau} = 0$ represents HFSBs that are neutrally-buoyant on average.

The three plots in Fig. 8 are organized in the same manner as those in Fig. 6. The three trends in each plot do not show much deviation from each other, suggesting that the flow rate of BFS does not have a
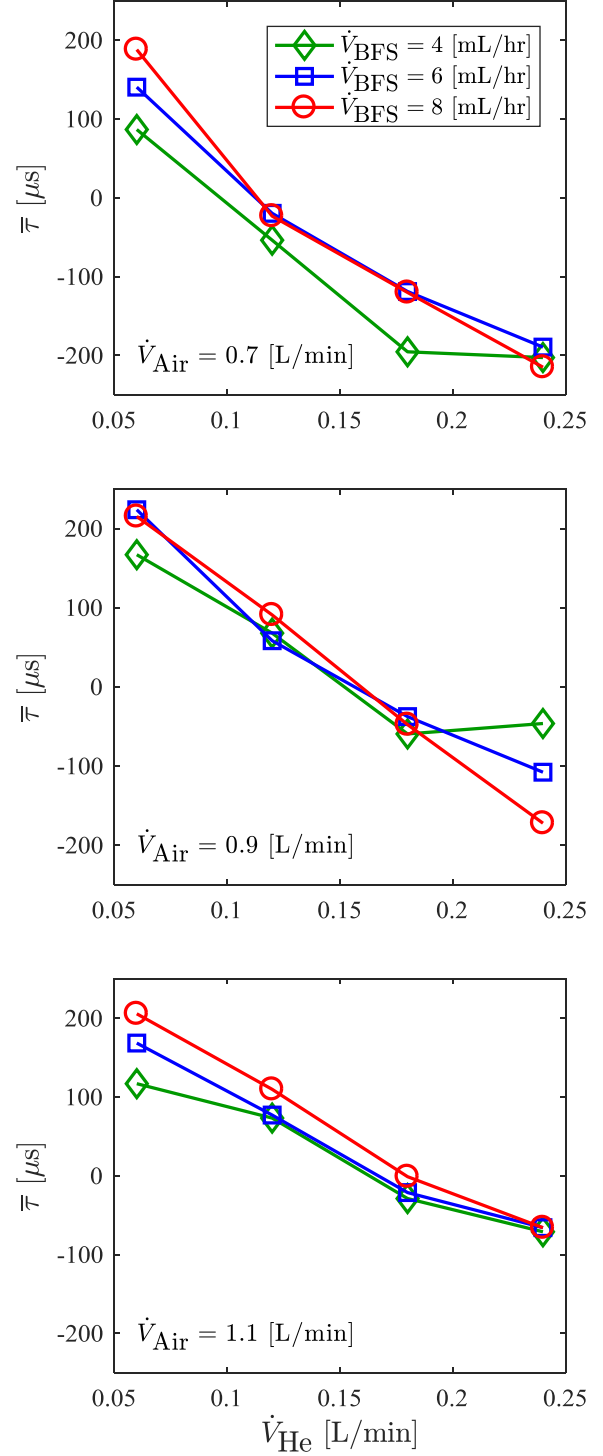

Fig. 8 Mean time response ($\bar{\tau}$) for all 36 nozzle input combinations. Each point represents the average for all τ calculated in the region $-0.5d \leq x \leq 0$ along the stagnation streamline using the mean velocity fields following Eq. 1.

significant impact on the mean time response of the HFSBs. The flow rate of air into the nozzles also does not seem to have a large impact on the mean time response, but a slight shift of the trends upwards is visible as $\dot{V}_{air}$ is increased. The most significant variation in time response occurs as helium flow rate is altered, and this variation is nearly linear. The large changes in τ with increasing $\dot{V}_{He}$ are expected because it is the amount of helium within the bubble that will have the largest impact on its overall density. With respect to Eq. 1, a positive time response indicates that a particle is heavier than the surrounding fluid, while a negative time response represents a particle that is buoyant. Fig. 8 reveals that increasing helium flow reduces the time response of the HFSBs, eventually leading to the production of buoyant HFSBs on average.

An important characteristic of the trends in Fig. 8 is that each of them passes through $\bar{\tau} = 0$. This indicates that the helium flow rate can be varied to achieve HFSBs that are neutrally-buoyant on average for all present combinations of air and BFS into the nozzles. The result found here that is closest to $\bar{\tau} = 0$ occurs for $\dot{V}_{BFS} = 8$ mL/hr, $\dot{V}_{He} = 0.18$ L/min, and $\dot{V}_{Air} = 1.1$ L/min, and corresponds to $\bar{\tau} = -1$ μs. This combination of nozzle input flow rates will be considered the optimal case from here forward, and is the same operating point used in Fig. 7 to display the distribution of HFSB diameters from 8 nozzles.

Although the optimal case results in HFSBs that are nearly neutrally-buoyant on average, the distribution of τ must be determined to know the range of time responses that can be expected when operating the full-scale system. This has been done using Eq. 1 once again. The mean velocity fields from applying the sum-of-correlation technique to the 1-μm fog particles were used as the velocity reference u, and u' was obtained from individual particle tracks from the time-resolved 2D PTV processing. The spatial derivative of u' has been calculated by applying a least-squares optimal quadratic fit with a kernel size of 5. Eq. 1 was applied to each particle track for all available data in the range $-0.5d \leq x \leq 0$, and the results were averaged to obtain one value for τ from each track. To obtain more samples, all tracks within a 5-mm window centered on the stagnation streamline were considered. The resulting distribution of time responses can be viewed in Fig. 9. The values for τ are normally distributed with a standard deviation of 179 μs, and this is expected to be a slight overestimate caused by the slight unsteadiness in the flow. This
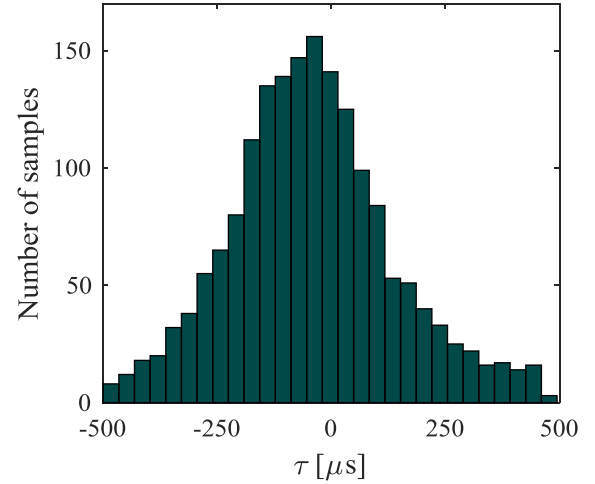
Fig. 9 Distribution of HFSB time responses (τ) at the optimal operating point of the system.

standard deviation is much larger than the standard deviation of 20 μs reported by Engler Faleiros et al. (2018). The larger deviation in τ is a result of the wide range of bubble sizes produced by the full-scale system.

Considering the distribution in Fig. 9, the HFSBs produced at the optimal operating point can be expected to have a time response of a few hundred microseconds. This must be accounted for when designing an experiment using the present HFSB generator. It is necessary to ensure that the characteristic time scale of the flow is at least an order of magnitude larger than the time response of the seeding particles for accurate flow measurements (Tropea et al. 2007). The present particles will therefore accurately trace velocity fluctuations in flows with characteristic time scales of approximately 5 ms or greater.

Comparing the trends in Fig. 6 and 8, it is evident that HFSBs with similar mean diameters can have significantly different mean time responses. This suggests that bubble diameter is not the only factor that determines the time response. More specifically, the diameter increase due to BFS seems to cause negligible differences in relaxation time compared to the diameter increases associated with helium flow.
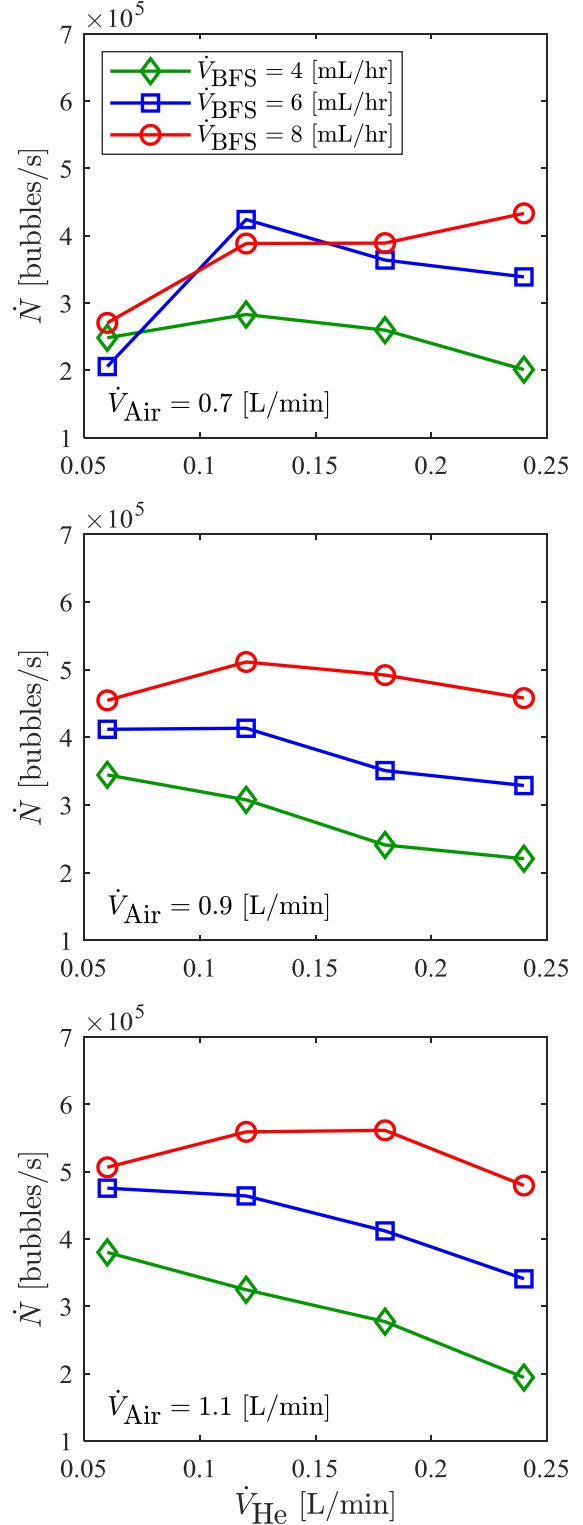
4.3 Production Rates and Seeding Density

The total production rate of the HFSB generator will be denoted as $\dot{N}$ and has been determined using the snapshots of the streamtube cross-section outlined in

Section 3.3. With the effective laser sheet thickness (3 mm) and wind tunnel velocity (10.3 m/s) known, counting the particles within these images allows for estimating the production rate of the system given that the images cover the entire streamtube cross-section. This information has been used to estimate $\dot{N}$ and the results are given in Fig. 10 with the same plot organization as before. It can be seen the trends for $\dot{V}_{Air}$ = 0.7 L/min do not follow those of the other air flow rates. This deviation has been caused by poor performance of the nozzles for extreme values of air and BFS rates. Experiments revealed large amounts of foam build-up at the nozzles when low $\dot{V}_{Air}$ and high $\dot{V}_{BFS}$ were coupled. The result is a lower production from the nozzle and even complete nozzle shutdown in some cases. As is evident in the plot, this was not an issue for $\dot{V}_{Air}$ = 0.9 and 1.1 L/min.

The general trends in Fig. 10 reveal that BFS has the greatest impact on production rates by far. Increasing $\dot{V}_{BFS}$ increases $\dot{N}$ in all cases with proper nozzle operation, and some cases exhibit doubling of $\dot{N}$ when $\dot{V}_{BFS}$ is doubled. This suggests that BFS is a limiting factor for HFSB production rates and increasing beyond the 8 mL/hr studied here may result in even greater HFSB production from the present generator.

The maximum production rate of HFSBs occurs at the same flow rate combination that produced the optimal mean relaxation time of $\bar{\tau} = -1$ μs and results in the production 560,000 bubbles/s from the 8 nozzles. This corresponds to 70,000 bubbles/s from each nozzle, and the minimum production rate measured was approximately 19,000 bubbles/s from each nozzle. The maximum production rate per nozzle measured here is 40% larger than that of previous literature, which reports approximately 50,000 bubbles/s (Caridi et al. 2016).

Seeding density is critical when conducting large-scale volumetric measurements using correlation-based techniques. The seeding density produced by the present HFSB generator covers a cross-section of 15×15 cm^2. The seeding of the edges of the streamtube cross-section is inconsistent, and so this 15×15 cm^2 segment has been chosen to represent the centre of the streamtube where the seeding is more stable. The average number of particles within this region has been counted and divided by the known effective volume (15×15×0.3 cm^3) of the laser sheet segment to determine seeding density for each of the 36 operating cases. This has resulted in maximum and minimum seeding densities of 1.6 and 0.6 bubbles/cm^3, respectively, at a free stream velocity of

Fig. 10 Estimated HFSB production rates ($\dot{N}$) from the full-scale system for all 36 nozzle input parameters considered.

10.3 m/s. The piston-cylinder system used by Caridi et al. (2016) achieved a seeding density of 1 bubble/cm^3 in a wind tunnel experiment at 8.5 m/s with a similar streamtube cross-section of 15×20 cm^2. This evaluation highlights the need for placing a larger number of nozzles in series within each module to supply enough particles at higher velocities.

5 Summary and Conclusions

The present investigation focused on the development and characterization of a HFSB generator that is capable of producing sufficient seeding for particle velocimetry measurements in a wind tunnel environment. The HFSB generator is modular and based around the use of 3D-printed components, readily available parts, and standard lab equipment. The details of the system were outlined and fully characterized in a wind tunnel at 10.3 m/s. The modular design of the system allows for the customization of the HFSB streamtube cross-sectional dimensions and seeding density by adding modules in parallel and by arranging nozzles in series within a module, respectively. The honeycomb-like structure of the system ensures reduced upstream flow disturbances. Two modules each with 4 nozzles were utilized in the present full-scale system.

Bubble size, tracing fidelity, production rates, and seeding density were measured using shadowgraphy, PIV, PTV, and laser-based imaging experiments within the wind tunnel test section. How these characteristics change with varying air, helium, and BFS flow rates into the system was determined using 36 operating cases. It was found that the flow rate of air into the system does not have a significant impact on the tracing fidelity or bubble size, but it does act to regulate the overall performance of the nozzles. Low flow rates of air were shown to cause the nozzles to sputter and produce foam, resulting in lower production rates overall. The rate of BFS into the system determined the overall HFSB production rates. In some cases, doubling $\dot{V}_{\mathrm{BFS}}$ resulted in twice the production rate of HFSBs, indicating that BFS is a limiting factor. The results suggest that higher production rates than what were measured here can be achieved by further increasing the flow rate of BFS into the system. Finally, the amount of helium into the system was shown to be the primary determinant of tracing fidelity and bubble size. Tuning the helium flow rate allows for manipulation of the mean bubble diameter and mean particle time response, allowing for the production of HFSBs that are neutrally-buoyant on average.

The optimal operating case occurred at $\dot{V}_{\mathrm{BFS}} = 8$ mL/hr, $\dot{V}_{\mathrm{He}} = 0.18$ L/min, and $\dot{V}_{\mathrm{Air}} = 1.1$ L/min (per nozzle). The resulting HFSBs had a mean time response of -1 μs and a mean diameter of 0.46 mm. However, the distribution of particle sizes was quite broad with a standard deviation of 23% (0.10 mm), leading to a standard deviation of 179 μs for the time response. This deviation in bubble sizes may be attributable to the difficulties associated with operating multiple nozzles at once using single sources of air and helium, or the fact that the nozzles are operating downward into a cross-flow. Preliminary experiments using a single nozzle resulted in a much narrower distribution of bubble sizes, but the use of many nozzles is critical for reaching the high production rates required for wind tunnel experiments. Improvements to the distribution system will likely result in the production of HFSBs with a narrower distribution of sizes and therefore a more consistent time response. Considering the distribution of time responses obtained at the optimal operating point, the present system can be used to measure flow features with a time scale of 5 ms or greater with negligible error.

The aforementioned optimal operating case resulted in the highest production rate of HFSBs. This value is roughly 560,000 bubbles/s from the 8-nozzle system, or 70,000 bubbles/s from each nozzle. The results also indicate that higher rates can be achieved with the current nozzles with a further increase of BFS. The outer edges of the streamtube that was produced by the two-module system had inconsistent seeding; however, the centre region was more stable. The stable region had an area of 15×15 cm^2, and the seeding density within this region was 1.6 bubbles/cm^3 at 10.3 m/s. Adding more nozzles within the modules will allow for obtaining higher seeding densities, and adding modules in parallel will allow for manipulation of the streamtube cross-sectional area.

References

Babie BM, Nelson RC (2010) An experimental investigation of bending wave instability modes in a generic four-vortex wake. Phys Fluids 22:077101

Biwole PH, Yan W, Zhang Y, Roux JJ (2009) A complete 3D particle tracking algorithm and its application to the indoor airflow study. Meas Sci Technol 20:115403

Bosbach J, Kühn M, Wagner C (2009) Large scale particle image velocimetry with helium filled soap bubbles. Exp Fluids 46:539-547

Caridi GCA, Ragni D, Sciacchitano A, Scarano F (2016) HFSB-seeding for large-scale tomographic PIV in wind tunnels. Exp Fluids 57:190

Caridi GCA, Sciacchitano A, Scarano F (2017) Helium-filled soap bubbles for vortex core velocimetry. Exp Fluids 58:130

Elsinga GE, Scarano F, Wieneke B, van Oudheusden BW (2006) Tomographic particle image velocimetry. Exp Fluids 41:933-947

Engler Faleiros D, Tuinstra M, Sciacchitano A, Scarano F (2018) Helium-filled soap bubbles tracing fidelity in wall-bounded turbulence. Exp Fluids 59:56

Hale RW, Tan P, Stowell RC, Ordway DE (1971) Development of an integrated system for flow visualization in air using neutrally-buoyant bubbles. SAI-RR 7107, SAGE ACTION Inc, Ithaca NY

Huhn F, Schanz D, Gesemann S, Dierksheide U, van de Meerendonk R, Schröder A (2017) Large-scale volumetric flow measurement in a pure thermal plume by dense tracking of helium-filled soap bubbles. Exp Fluids 58:116

Kerho MF, Bragg MB (1994) Neutrally buoyant bubbles used as flow tracers in air. Exp Fluids 16:393-400

Kühn M, Ehrenfried K, Bosbach J, Wagner C (2011) Large-scale tomographic particle image velocimetry using helium-filled soap bubbles. Exp Fluids 50:929-948

Meinhart CD, Wereley ST, Santiago JG (2000) A PIV algorithm for estimating time-averaged velocity fields. J Fluids Eng 122:285-289

Müller D, Müller B, Renz U (2001) Three-dimensional particle-streak tracking (PST) velocity measurements of a heat exchanger inlet flow. Exp Fluids 30:645-656

Raffel M, Willert CE, Wereley ST, Kompenhans J (2007) *Particle Image Velocimetry: A Practical Guide*. Springer, Berlin, Germany

Scarano F (2013) Tomographic PIV: principles and practice. Meas Sci Technol 24:012001

Scarano F, Ghaemi S, Caridi GCA, Bosbach J, Dierksheide U, Sciacchitano A (2015) On the use of helium-filled soap bubbles for large-scale tomographic PIV in wind tunnel experiments. Exp Fluids 56:42

Schanz D, Gesemann S, Schröder A (2016). Shake-The-Box: Lagrangian particle tracking at high particle image densities. Exp Fluids 57:70

Schneiders JFG, Caridi GCA, Sciacchitano A, Scarano F (2016) Large-scale volumetric pressure from tomographic PTV with HFSB tracers. Exp Fluids 57:164

Terra W, Sciacchitano A, Scarano F (2017) Aerodynamic drag of a transitioning sphere by large-scale tomographic-PIV. Exp Fluids 58:83

Tropea C, Yarin AL, Foss J (2007) *Handbook of Experimental Fluid Mechanics*. Springer, Berlin, Germany